An atomic probe of dark matter differential interactions with elementary particles

Yossi Rosenzweig,* Yevgeny Kats,* Menachem Givon, Yonathan Japha, and Ron Folman
Department of Physics, Ben-Gurion University of the Negev, Israel

Searching for physics beyond the Standard Model is one of the main tasks of experimental physics. Candidates for dark matter include axion-like ultralight bosonic particles. Comagnetometers form ultra-high sensitivity probes for such particles and any exotic field that interacts with the spin of an atom. Here, we propose a multi-atom-species probe that enables not only to discover such fields and measure their spectrum but also to determine the ratios of their coupling strengths to sub-atomic elementary particles, electrons, neutrons and protons. We further show that the multi-faceted capabilities of this probe may be demonstrated with synthetic exotic fields generated by a combination of regular magnetic fields and light-induced fictitious magnetic fields in alkali atoms. These synthetic fields also enable the accurate calibration of any magnetometer or comagnetometer probe for exotic physics.

arXiv:2312.05894v1 [hep-ph] 10 Dec 2023

Searching for physics beyond the Standard Model (BSM) is one of the main tasks of experimental physics if we are to explain yet ill-understood phenomena such as the strong CP problem [1], neutrino oscillations [2, 3], matter-antimatter asymmetry [4], dark energy [5, 6], dark matter (DM) [7, 8], and the period of cosmic inflation [9–12] and what preceded it. One class of BSM scenarios that can be probed with comagnetometers is dark matter in the form of axion-like particles (ALPs) [13]. These are light spin-0 particles that arise generically as pseudo-Nambu-Goldstone bosons of spontaneously broken global symmetries. They are commonly long-lived and can be produced in the right amount during the cosmological evolution of the universe to account for the observed DM abundance. For ALP masses $m_a \ll 1$ eV, these ultra-light bosonic particles will have high occupation numbers and behave as a classical field oscillating with frequency $f \simeq m_a/(2\pi)$. One of the strong motivations for ALPs is the QCD axion – a hypothetical particle naturally emerging from a solution to the strong CP problem [1, 14]. While the simplest DM scenarios would require the QCD axion to be too heavy to be probed with comagnetometers, there exist scenarios in which a much lighter QCD axion can naturally produce the observed DM abundance [15–17].

There are several ways or "portals" for ALPs to access the Standard Model particles [8, 18]. In particular, they would, in many cases, couple to Standard Model fermion fields ψ via an interaction term of the form

$$\mathcal{L} = \frac{g_f}{f_a}\,\partial_\mu a\,\bar{\psi}\gamma^\mu\gamma^5\psi\,, \tag{1}$$

where a is the ALP field, f_a is the spontaneous symmetry-breaking energy scale, and g_f is a model-dependent and fermion-dependent coupling factor (analogous to charge and dimensionless in $\hbar = c = 1$ units). There are several ongoing experiments with the goal of detecting such an interaction [19–21]. A pertinent aspect is that in the nonrelativistic limit, one obtains an interaction that is analogous to the interaction of a spin with a magnetic field, and follows the Hamiltonian:

$$\mathcal{H} \approx -\frac{g_f}{f_a}\frac{\mathbf{S}}{|S|}\cdot\nabla a\,, \tag{2}$$

where $\mathbf{S}$ is the fermion spin ($|S| = 1/2$ is the maximum spin projection), and ∇a is the spatial gradient of the ALP field. While the couplings g_f in the simplest QCD axion models are commonly $\mathcal{O}(1)$, which would make the effect extremely small, there exist scenarios in which they are enhanced exponentially [22]. Relevant in particular in the context of this work are scenarios in which the couplings to electrons are enhanced relative to couplings to nucleons, such as one of the scenarios in Ref. [22]. The ALP couplings to electrons and neutrons are subject to constraints from star cooling [23] and neutron star cooling [24], respectively. These bound the possible signal size from a galactic ALP DM halo, making it challenging for comagnetometers to observe. However, if the ALP DM is not homogeneous but forms ALP stars that the Earth encounters once in a while, or produces a halo around the Sun, its signals can be detectable. Domain walls of the ALP field are another possible target for comagnetometers. These and additional possibilities are reviewed in Ref. [25].

Currently, comagnetometers are becoming the sensor of choice for testing ALP-fermion interaction theories [26–29] due to their high sensitivity, relative simplicity, and their unique feature of attenuating low-frequency magnetic fields [30] while keeping their sensitivity to spin interactions with exotic fields [31]. A comagnetometer comprises an alkali vapor and a noble gas with a non-zero nuclear spin confined in a glass cell. A pump laser polarizes the alkali vapor along the axis of the beam (z-axis, see Fig. 5 in the appendix), which polarizes the noble gas via spin-exchange collisions along the same axis [32]. Typically, a second alkali is added to increase the noble gas's pumping efficiency and the probed alkali's polarization homogeneity [33], but for simplicity, we will neglect this third species as it has little impact on the fundamental physics. The cell is heated to have a high vapor density

* These two authors contributed equally.

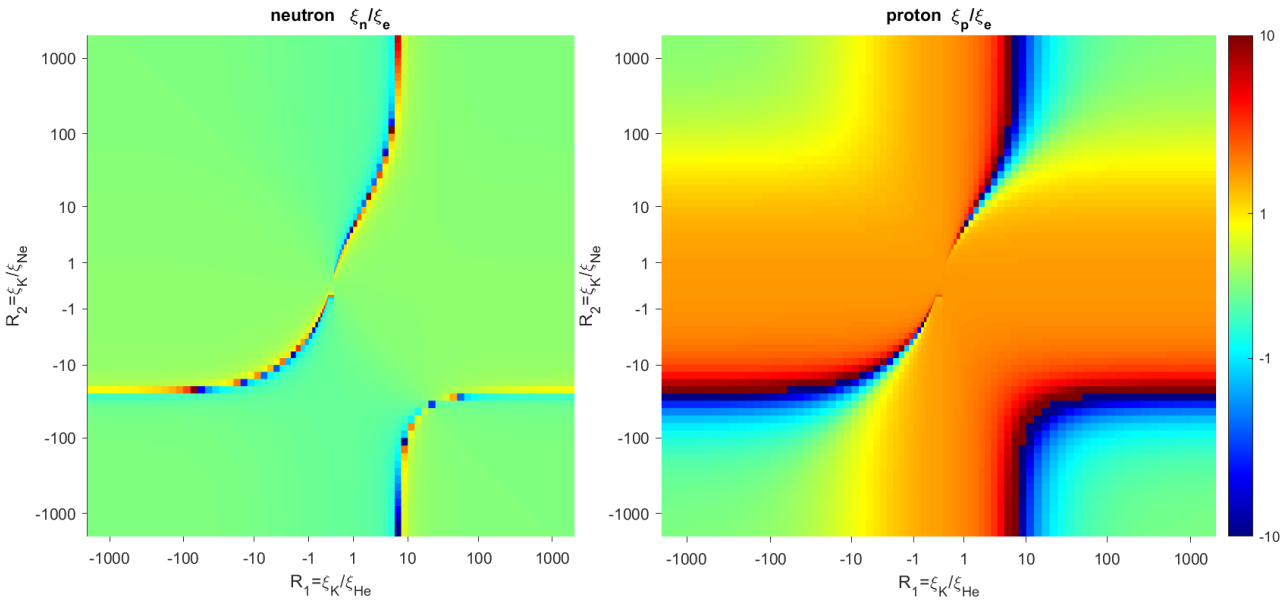

FIG. 1. Coupling constants of the ALP field with neutrons ξ_n (left) and protons ξ_p (right) in units of the coupling with electrons ξ_e deduced from two atomic coupling ratios $\mathcal{R}_N = \xi_A/\xi_N$ with the same alkali atom ($A = {}^{39}$K) and two different noble gas atoms ($N = {}^{3}$He, ^{21}Ne). The atomic coupling ratio is obtained from simultaneous measurements in two comagnetometers with the same atomic species but different operation parameters. The values of the sub-atomic elementary particle coupling constants are calculated using nuclear spin-contents for the alkali and noble-gas atoms, as given in Table II in the Appendix. To emphasize variations of the nucleon coupling within the range -10 to 10, values below and above this range are represented by the blue and red colors at the edge of this range. Most of the points in the $\mathcal{R}_1$–$\mathcal{R}_2$ plane require the coupling to protons to be larger than to neutrons because the proton spin fractions in both noble gases according to the models from Table II are small. All the values $\mathcal{R}_N$ can be simulated by a synthetic exotic field produced with a combination of a regular and fictitious light-induced magnetic fields.

and placed inside a magnetic shield. A linearly polarized probe laser beam is sent along the x-axis and measures the spin projection along this axis. If there were no noble gas, a magnetic field along the y-axis would cause the spin to precess in the x-z plane and be detected by the probe beam [34]. When the polarized noble gas is added, the alkali atoms are affected by the magnetic field induced by the polarized gas. This field can be countered by applying an external magnetic field equal in amplitude but with an opposite sign ("compensation field"). Now the net field affecting the alkali is zero, as we had before the addition of the polarized noble gas, but with a major difference: The polarized noble gas will follow a slowly varying transverse magnetic field (with respect to the pump and probe axes), causing the net magnetic field sensed by the alkali to remain (close to) zero, effectively attenuating magnetic field noise. The latter makes the comagnetometer a leading probe for BSM spin interactions, as it attenuates the low-frequency response to regular magnetic fields but not to pseudo-magnetic exotic fields that presumably interact with spins via different couplings.

Unlike the magnetic field, which interacts with the electron and nucleon spins with coupling strengths given by their magnetic moments, the ALP exotic field can couple to the electron, proton and neutron spins with unknown arbitrary strengths. Coupling to the electronic spin affects only the alkali atoms, which have non-zero electronic spin, while coupling to nuclear spin would mainly affect the magnetization in the vapor cell due to noble gas in the comagnetometer, whose density is much larger than that of the alkali gas. Furthermore, coupling to the nucleons will also affect the spin of the alkali through the large magnetic field induced by the polarized noble gas on the alkali. An exotic field coupling ratio between the coupling to the electron and nucleon spins that is significantly different from that of the magnetic field, would evade the compensation effect and lead to a strong response from the comagnetometer. We briefly note that for the magnetic shielding to not attenuate exotic fields that couple to the electron spin, one should use shielding whose operation is based on electric current (conductors or superconductors) rather than spin (soft ferromagnets or ferrimagnets) [35].

While detecting a signal related to ALP exotic fields can reveal the field's existence and some of its spectral properties, it cannot determine the absolute amplitude of this field because the coupling of the field to the atoms is not known. Furthermore, coupling to the atoms depends on the atom's specific nuclear and electronic structure. By detecting a signal in a single comagnetometer, it is impossible to determine the coupling constants of the exotic

field with the elementary sub-atomic particles or the coupling to each of the atomic species. Here, we propose a scheme that uses simultaneous detection in a few comagnetometers, some of them with different atomic species, to determine the ratios of coupling constants to the elementary fermions. We further show that this scheme can be readily demonstrated with the help of a synthetic exotic field.

In addition, we describe how the synthetic field may also be used to calibrate the comagnetometers. Calibration is a major problem in BSM searches because one cannot generate a calibration field for sensors that have not yet detected a real signal. Recently, it was proposed to calibrate a comagnetometer by comparison of a detailed theoretical model to the frequency-dependent measurements of a magnetic field [36]. However, magnetic fields always interact with the electronic and nuclear spins of atoms with the same coupling strength ratio related to their magnetic moments and, therefore, cannot be used directly to calibrate the response of the comagnetometers to fields that may interact with the spins in a completely different way.

We begin by presenting in Fig. 1 an example of the output of the new probe, namely the determination of the ratios of the different fundamental couplings between the exotic field and the elementary sub-atomic particles. The coupling constants $\xi_f \equiv g_f/f_a$ of the exotic field to the sub-atomic fermions ($f = e, n, p$ for electrons, neutrons and protons) are not known and may be extracted from atomic measurements using comagnetometers. However, a single measurement in an atomic comagnetometer cannot reveal these constants because each comagnetometer uses two atomic species: alkali atoms and noble gas atoms and the coupling of the exotic field to each of the atomic species is a weighted sum over its couplings to the sub-atomic particles. In particular, the coupling to the nucleus of a given atom is given by $\xi_{\rm nuc} = \sigma_n \xi_n + \sigma_p \xi_p$, where σ_n and σ_p are the fractional contributions due to neutron and proton spins to the spin of the specific nucleus. In our scheme, we first extract the ratio $\mathcal{R}_N \equiv \xi_A/\xi_N$ of the coupling of the exotic field with the alkali atoms (A) and the noble gas atoms (N) used in a pair of comagnetometers with the same atomic constituents. Then, by taking the results of such a ratio from two pairs of comagnetometers using different atomic species we can also extract the coupling ratios ξ_n/ξ_e and ξ_p/ξ_e of the elementary subatomic particles, as demonstrated in Fig. 1.

Let us now detail how a synthetic field enables a direct way to demonstrate, calibrate, and optimize the comagnetometer response to ALP-electronic/nuclear spin interaction, and utilize this understanding to explain how the suggested novel probe enables the measurement of the fundamental couplings. Using a laser to apply an oscillating electric field near the alkali optical resonance results in an AC Stark shift for the alkali, which manifests itself as a fictitious magnetic field via the vector polarizability [37], while this field does not exist for noble gas as the latter has only scalar polarizability [38]. In addition, the laser field frequency is tuned near the resonance frequency of a given alkali atomic species and therefore affects mainly these atoms. This makes the light-induced fictitious magnetic field indistinguishable from an exotic field that couples only to the alkali spin. Generating a synthetic field that couples only to the nuclei of the noble gas is also possible in a comagnetometer by applying a magnetic field and compensating its effect on the alkali by generating an equal and opposite light shift fictitious magnetic field. This way, the magnetic field affects only the polarized noble gas, mimicking the effect of exotic field coupling only to the noble gas nucleus. A general model with an arbitrary ratio between the coupling factors of the exotic field to the spins of the alkali and the noble gas can be tested using a combination of regular and fictitious light-induced magnetic fields. Figure 5 in the appendix depicts the proposed experimental setup. We note that generating synthetic fields by non-magnetic spin interaction with different coupling strengths to electronic and nucleon spins can also be used in atomic magnetometers without the polarized nucleus of a noble gas, but a comagnetometer is preferred due to its high sensitivity, its ability to attenuate the response to magnetic fields and the variability of its response to different coupling ratios of exotic fields to fermions.

We now put the synthetic field and all other interactions into one equation. Specifically, the dynamics due to the interaction of the spins of the gases (n_g species) with the magnetic, exotic and optical fields and the interaction between the spins is described by the set of Bloch equations for the polarizations $\mathbf{P}_j$ of the different species ($1 \le j \le n_g$)

$$\dot{\mathbf{P}}_j = \frac{1}{q_j}\left\{\left[\gamma_j\left(\mathbf{B} + \sum_k \lambda_{jk} M_0^k \mathbf{P}_k + \mathbf{L}_j\right) + \xi_j \mathbf{b}\right] \times \mathbf{P}_j + \sum_k \kappa_{jk} n_k (\mathbf{P}_k - \mathbf{P}_j) - R_{pj}(\mathbf{P}_j - \mathbf{s}) - \Gamma_j \mathbf{P}_j\right\}, \tag{3}$$

where we sum over all existing species (index k). $\mathbf{P}_j$ are normalized to a maximal length of unity, $\mathbf{B}$ is the magnetic field vector, and $\mathbf{L}_j$ is the fictitious magnetic field (AC Stark shift) due to the interaction between the laser light field and the atoms. Here γ_j are the gyromagnetic ratios: electron gyromagnetic ratio γ_e for the alkali atoms, γ_N for the nuclear spin of the noble gas, and q_j are the nuclear slowing-down factors for the alkali atoms and 1 for the noble gas. The pseudo magnetic field due to an exotic field interaction, $\mathbf{b}$, is proportional to the exotic field gradient ∇a. It couples to the atoms via the constants ξ_j, representing the coupling to the electronic and nuclear spins of each species. These coupling factors emerge from the coupling strengths g_e/f_a, g_p/f_a and g_n/f_a for the exotic field interaction with the spin of the electrons, protons and neutrons in the atoms [39]. In addition to the coupling to external fields, each species

j experiences an effective magnetic field induced by the magnetization of each of the other species k through the coupling factors λ_{jk}, which include a geometrical and temperature-dependent enhancement factor. The magnetization is proportional to the normalized polarization $\mathbf{P}_k$ and the maximal magnetization $M_0^k = \mu_k n_k$ where n is the density and μ is the magnetic moment of the atom k. The second line of Eq. (3) includes the incoherent processes: laser pumping with a rate R_{pj} (typically $R_{pj} \neq 0$ only for one alkali gas) and direction unit vector $\mathbf{s}$, spin exchange with a rate proportional to κ_{jk} [33] and Γ_j accounts for all the remaining relaxation processes for species j.

Here we are interested in the steady-state solution of the coupled Bloch equations in response to a monochromatic exotic field. A method for obtaining this solution for an arbitrary number of species is given in the appendix. We consider the simple case of two species: a single alkali gas ($j \to A$, specifically potassium) and a noble gas ($j \to N$, specifically ^{3}He or ^{21}Ne). The specific parameters of the model system are given in Table I in the appendix. The coupling constant ξ_N of the noble gas to the exotic field is solely due to the interaction of the exotic field with the proton and neutron spins. On the other hand, the coupling constant ξ_A of the alkali atom with the exotic field may have an electronic and nuclear contribution.

In Fig. 2, we present the steady-state response to a transverse (with respect to the pump axis) magnetic field perturbation as a function of the perturbation frequency. At low frequencies, the response is attenuated by the mechanism described above. The same response is expected for a pseudo magnetic exotic field if $\xi_A/\xi_N = \gamma_e/\gamma_N$, such that the exotic field mimics a magnetic field. However, in the general case the two coupling constants may have an arbitrary ratio $\mathcal{R}_N \equiv \xi_A/\xi_N$ and the response is then expected to be much stronger if $\mathcal{R}_N \neq \gamma_e/\gamma_N$. It is interesting to note that the attenuation near $\mathcal{R}_N = \gamma_e/\gamma_N$ is bigger than for exactly $\mathcal{R}_N = \gamma_e/\gamma_N$ as the signal due to exotic field coupling to the electron is out of phase from the signal due to exotic coupling to the nucleon [31], resulting in a destructive interference. Alternatively, near $\mathcal{R}_N = -\gamma_e/\gamma_N$ there could be an increase in the signal as the transverse component of the noble gas does not compensate for the field affecting the alkali but actually adds to it, resulting in an increase in signal at that value. Those features, and others can be seen in Fig. 3 where we show the steady-state response of the system to an exotic field perturbation with a frequency of 1 Hz along the y-axis of the setup, as a function of the ratio $\mathcal{R}_N$ between the exotic field coupling to the alkali and noble gas.

Now that we have covered all the basic elements, we are able to show how the multi-atom-species probe works. The interaction of ALP-fields involves three unknown coupling parameters: ξ_e, ξ_p and ξ_n for the interaction with electrons, protons and neutrons. A single-frequency measurement of a comagnetometer with given

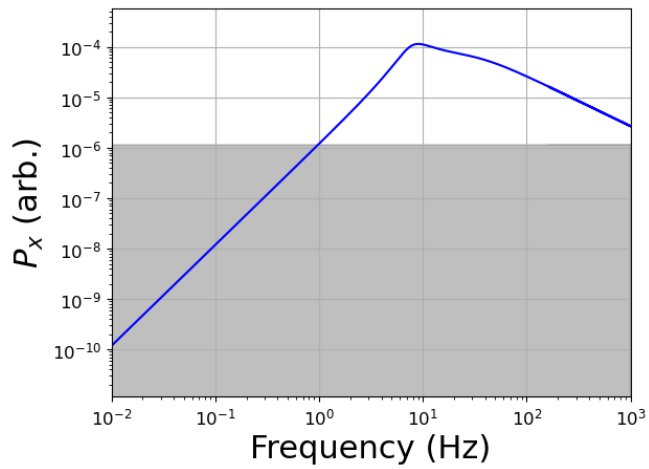

FIG. 2. Response of a ^{39}K-^{3}He comagnetometer to a (weak) 1 pT magnetic field oscillating with frequency f. The magnetic field perturbation is along the y-axis, perpendicular to the pump and probe beams (Fig. 5). The response is the steady-state solution of Eq. (3) for the x component of the polarization of the probed alkali. The gray area represents polarization values below the minimal detectable value, which was taken to be the maximal polarization generated by an oscillating magnetic signal of 10 fT. It can be seen that low-frequency magnetic fields are attenuated as expected from a comagnetometer.

alkali and noble atoms may reveal the frequency of the exotic field but would teach us nothing about the amplitude of the field and the coupling strengths, which constitute four unknowns. For small perturbations, the response of the comagnetometer is linearly proportional to the field amplitude b_y of the exotic field. Let us now consider two comagnetometers with different response curves $P_x^j(\mathcal{R}_j, b_y)$, where P_x^j and $\mathcal{R}_j$, for $j = 1, 2$ represent the alkali polarizations and coupling ratios of the two comagnetometers. The ratio P_x^1/P_x^2 is independent of the field amplitude b_y. If the two comagnetometers have the same noble gas but different response curves due to different system parameters (such as gas pressures, pumping rates, etc.), then the ratio of the responses may reveal the value of the coupling ratio $\mathcal{R}_N$ for the nucleus of the noble gas. The response of different comagnetometers (and the ratio of their response) as a function of $\mathcal{R}_N$ can be experimentally simulated by a synthetic exotic field combined from the two applied fields L_y and B_y: For any given values of ξ_A (coupling to the alkali) and ξ_N (coupling to the noble gas) the following perturbations along the y-axis simulate an exotic field:

$$B_y = \frac{\xi_N}{\gamma_N} b_y \,, \tag{4}$$

$$L_y = \left(\frac{\xi_A}{\gamma_e} - \frac{\xi_N}{\gamma_N} \right) b_y \,. \tag{5}$$

The coefficients ξ_A and ξ_N are linear combinations of the fundamental coupling coefficients of the proton and

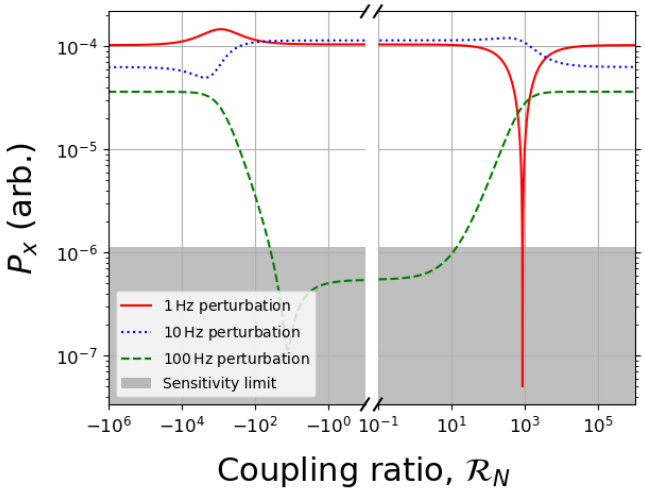

FIG. 3. Response of a ^{39}K-^{3}He comagnetometer to an exotic field perturbation of different frequencies as a function of the ratio between its coupling to the alkali and noble gas $\mathcal{R}_N = \xi_A/\xi_N$. The magnitude of the effective pseudo magnetic fields $b_A \equiv \xi_A b/\gamma_e$ and $b_N \equiv \xi_N b/\gamma_N$, corresponding to the coupling with the alkali and noble gas, was normalized to be $\sqrt{|b_A|^2 + |b_N|^2} = \sqrt{2}\,\mathrm{pT}$ for any value of $\mathcal{R}_N$ in order to keep the response as a function of $\mathcal{R}_N$ independent of the field strength, and that at $\mathcal{R}_N = \gamma_e/\gamma_N$ the exotic field will be equivalent to a 1 pT magnetic field. The gray area, as in Fig. 2, represents the range of values of P_x below the minimal detectable value.

neutron, with coefficients that depend on the specific nucleus [39], and in the case of ξ_A also of the electron. The ratio of the response of two comagnetometers as a function of $\mathcal{R}_N$ is depicted in Fig. 4 for two different pairs of comagnetometers with a different noble gas, such that the two comagnetometers in each pair have different response curves due to two different pumping rates: optimal and low (for details, see Table I in the appendix). We assume the alkali to be the same in all the comagnetometers only for simplicity of discussion. Simultaneous measurement of an exotic field signal in the four comagnetometers may enable the determination of the coupling ratios for the sub-atomic elementary particles. Measurement of $\mathcal{R}_{N_1}$ and $\mathcal{R}_{N_2}$ from the response ratios of two comagnetometers that share the same noble gas N_1 or N_2, respectively, may reveal the exotic field coupling ratios using the following equations:

$$\frac{\xi_e + (q_A - 1)(\sigma_p^A \xi_p + \sigma_n^A \xi_n)}{\sigma_p^{N_1} \xi_p + \sigma_n^{N_1} \xi_n} = \mathcal{R}_{N_1}\,, \tag{6}$$

$$\frac{\xi_e + (q_A - 1)(\sigma_p^A \xi_p + \sigma_n^A \xi_n)}{\sigma_p^{N_2} \xi_p + \sigma_n^{N_2} \xi_n} = \mathcal{R}_{N_2}\,, \tag{7}$$

where ξ_e, ξ_p and ξ_n are the exotic spin couplings to the electron, proton and neutron, respectively. The σ_p and σ_n are the fractions of the nuclear spin due to proton and neutron spins, respectively, in the alkali (A) or one of the noble gases ($N_{1,2}$) [39], whose values are given in Table II in the appendix. Solving the set of two equations would reveal the ratios g_p/g_e and g_n/g_e. In fact, a set of only three comagnetometers where one of them has a different noble gas is sufficient for determining these ratios, but the example of two pairs of comagnetometers is simpler to present. In Fig. 4, we show the ratios between the responses of two pairs of comagnetometers as a function of the ratio between the fictitious magnetic field perturbation L_y and the regular magnetic field perturbation B_y, which corresponds to the coupling ratios $\mathcal{R}_N$ of the noble gases used in the comagnetometers. These differential responses enable the output of the probe, as presented in Fig. 1.

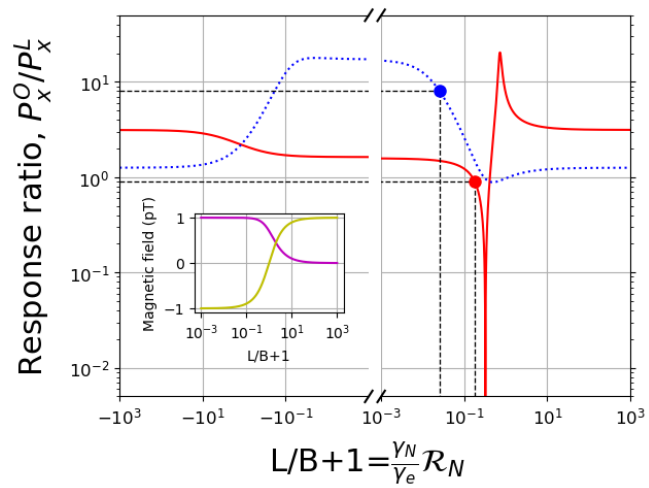

FIG. 4. Response ratios of different comagnetometers to a synthetic exotic field perturbation at 1 Hz as a function of the ratio between the light shift (L) and magnetic (B) fields in the system. The latter ratio is related to the ratio of exotic field coupling to the alkali and noble gas spin as $L/B + 1 = \frac{\gamma_N}{\gamma_e}\mathcal{R}_N$ [see Eqs. (4) and (5)]. The response ratios of a ^{39}K-^{3}He and a ^{39}K-^{21}Ne comagnetometers with optimal pumping rate, P_x^O, to a ^{39}K-^{3}He and a ^{39}K-^{21}Ne comagnetometers with a low pumping rate, P_x^L, are shown in solid red and dotted blue, respectively. The inset shows how each value of $\mathcal{R}_N$ can be synthetically generated by a combination of a light shift field and a magnetic field (yellow and magenta lines, respectively) using the experimental scheme in Fig. 5. The dashed black line shows a possible $\mathcal{R}_N$ measurement in each pair of the comagnetometers. By comparing the amplitude ratios of the exotic field signals measured simultaneously in the comagnetometers (see text) to the values appearing in these curves, the exotic coupling ratios can be found. While the same value of a response ratio can usually be obtained at two different points on the curve, this apparent ambiguity can be resolved by looking at the response ratio of a pair of comagnetometers with different noble gases (see Table III in the appendix).

As an outlook we note that in this work the analysis was made utilizing the magnitude of the response. However, the phase of a comagnetometer response to an exotic field perturbation also carries information [31] that can be utilized whether the two comagnetometers experi-

ence the same perturbation [40] or with a time delay. An additional future improvement would come from work narrowing the uncertainties concerning proton and neutron spin fractions in the different elements [39]. If theoretical models are not accurate enough, improvement of accuracy can be achieved by utilizing additional species of noble gas with different spin contents (e.g., ^{129}Xe).

ACKNOWLEDGMENTS

We thankfully acknowledge useful discussions with Dmitry Budker, Derek F. Jackson Kimball and Joshua Eby. This work was supported by the United States - Israel Binational Science Foundation (BSF) Grants No. 2016635 and 2018257, the Israel Science Foundation Grant No. 1666/22, and in part by the Israel Innovation Authority Grants No. 67082 and 74482. Y.R. thanks ELTA for financial support.

Appendix A

For any real Cartesian vector $\mathbf{a}$, we define a complex value

$$a_\perp \equiv a_x + i a_y. \tag{A1}$$

It follows that the transverse complex part of the vectorial product of two vectors is given by

$$(\mathbf{a}\times\mathbf{b})_\perp = i(-a_\perp b_z + a_z b_\perp), \tag{A2}$$

and

$$(\mathbf{a}\times\mathbf{b})_z = \frac{i}{2}(-a_\perp b_\perp^* + a_\perp^* b_\perp). \tag{A3}$$

Working on Eq. (3), let us first assume that the applied magnetic field and the pumping direction $\mathbf{s}$ are in the same direction, $\hat{z}$. Then, in the absence of additional perturbations, all the polarizations are in the same direction, and the steady-state solution ($\dot{P}_j = 0$) for Eq. (3) reads

$$R_{pj} = \sum_k \left[\left(\sum_{k'} \kappa_{jk'} n_{k'} + \Gamma_j + R_{pj}\right)\delta_{jk} - \kappa_{jk} n_k\right] P_z^k\,. \tag{A4}$$

This can be written in a matrix form as

$$\hat{K} P_z = R_p\,, \tag{A5}$$

and has the solution

$$P_z = \hat{K}^{-1} R_p\,. \tag{A6}$$

The equations for the transverse components of the polarization are then

$$\begin{aligned}\dot{P}_\perp^j \;=\; & i\frac{\gamma_j}{q_j}\left[-\bar{b}_\perp^j P_z^j - \sum_k \lambda_{jk} M_0^k P_\perp^k P_z^j + b_z^j P_\perp^j \right.\\ & \left. + \sum_k \lambda_{jk} M_0^k P_z^k P_\perp^j\right] + \frac{1}{q_j}\sum_k \kappa_{jk} n_k (P_\perp^k - P_\perp^j) - \\ & (\Gamma_j + R_{pj}) P_\perp^j\,.\end{aligned} \tag{A7}$$

where $\bar{b}_\perp^j \equiv B_\perp + L_\perp^j + \frac{\xi_j b_\perp}{\gamma_j}$ is the perpendicular component of the effective magnetic field acting on species j. This can be written in a matrix form

$$\dot{P}_\perp = \hat{A} P_\perp - i\frac{\gamma}{q}\bar{b}_\perp P_z, \tag{A8}$$

where the last term is a vector where each component is a product of the effective transverse field and the polarization in the longitudinal direction, and the matrix $\hat{A}$ is given by

$$\begin{aligned}\hat{A}_{jk} \;=\; & -i\frac{1}{q_j}\left\{\gamma_j P_z^j \lambda_{jk} M_0^k + \kappa_{jk} n_k + \right.\\ & \delta_{jk}\left[i\gamma_j\left(b_z^j + \sum_k \lambda_{jk} M_0^k P_z^k\right) - \right.\\ & \left.\left.\sum_k \kappa_{jk} n_k - \Gamma_j - R_{pj}\right]\right\}\,.\end{aligned} \tag{A9}$$

Let us now take the transverse field perturbation to be monochromatic with frequency ω

$$\bar{b}_\perp(t) = \bar{b}_\perp(0) e^{-i\omega t}\,. \tag{A10}$$

By assuming a similar time-dependence of the solution $P_\perp$ we obtain

$$-i\omega P_\perp = \hat{A} P_\perp - i\frac{\gamma}{q}\bar{b}_\perp P_z\,. \tag{A11}$$

The solution is then readily given by

$$P_\perp(\omega) = -[\hat{A} + i\omega\hat{1}]^{-1}\frac{\gamma}{q}\bar{b}_\perp P_z\,. \tag{A12}$$

The polarization vector in response to a transverse field with frequency ω is

$$\mathbf{P}(t) = \mathbf{P}_+ e^{i\omega t} + \mathbf{P}_- e^{-i\omega t}\,, \tag{A13}$$

where $\mathbf{P}_\pm$ are complex. The actual polarization vectors are

$$\mathbf{P}_x = \mathbf{Re}\{\mathbf{P}\}\,, \quad \mathbf{P}_y = \mathrm{Im}\{\mathbf{P}\}\,. \tag{A14}$$

It follows that the amplitudes of the response to an input magnetic field with a given amplitude are

$$\sqrt{2\langle \mathbf{P}_{x,y}^2\rangle} = \frac{1}{2}|\mathbf{P}_+ \pm \mathbf{P}_-^*|\,. \tag{A15}$$

The $+$ and $-$ signs refer to the x and y components, respectively (defined with an input field in the x direction). The phases of the output signals with respect to the input signal are given by the argument of the respective complex quantities

$$\phi_{x,y} = \arg\{P_+ \pm P_-^*\}\,. \tag{A16}$$

The following parameters in Table I were used for generating Figs. 2, 3 and 4.

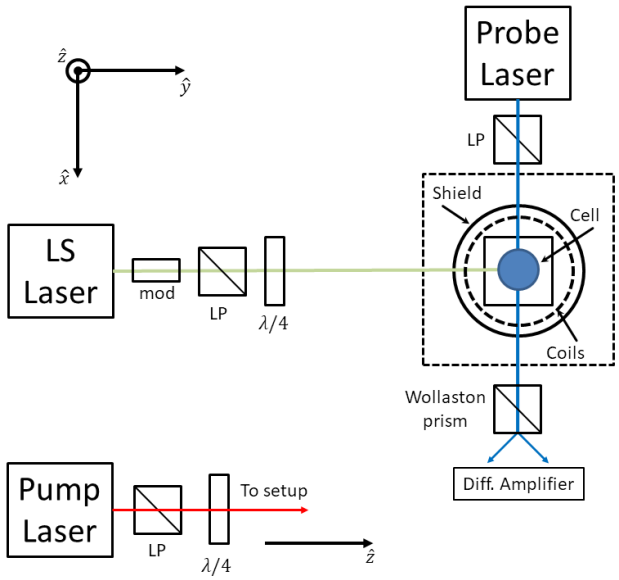

FIG. 5. Schematics of the experimental setup generating a synthetic exotic field in a comagnetometer. A pump laser propagating along the z-axis is circularly polarized using a linear polarizer (LP) and a quarter-wave plate ($\lambda/4$) and tuned to the alkali resonance. A linearly polarized probe beam laser is detuned from the alkali resonance and propagates along the x-axis. A light-shift laser (LS laser) is detuned from the alkali resonance and propagates along the y-axis. The LS laser is circularly polarized and is frequency-modulated using an EOM modulator (mod). After traversing the vapor cell, the probe beam polarization angle is measured using a Wollaston prism and a differential amplifier (Diff. Amplifier). The vapor cell (Cell) is placed inside a magnetic shield (Shield), and a set of coils (Coils) are added to nullify any residual magnetic field, including the magnetic field induced by the polarized atoms. By choosing a proper value of the light shift field and magnetic field (see text), it is possible to synthetically generate exotic fields with a different coupling to the electron and nucleus, allowing us to directly and accurately measure the system sensitivity to authentic exotic fields.

[1] R. D. Peccei and H. R. Quinn, CP conservation in the presence of pseudoparticles, Physical Review Letters **38**, 1440 (1977).

[2] Q. R. Ahmad *et al.*, Measurement of the Rate of $\nu_e + d \rightarrow p + p + e^-$ Interactions Produced by ^8B Solar Neutrinos at the Sudbury Neutrino Observatory, Physical Review Letters **87**, 071301 (2001).

[3] V. Barger, D. Marfatia, and K. Whisnant, *The physics of neutrinos* (Princeton University Press, 2012).

[4] L. Canetti, M. Drewes, and M. Shaposhnikov, Matter and antimatter in the universe, New Journal of Physics **14**, 095012 (2012).

[5] P. J. E. Peebles and B. Ratra, The cosmological constant and dark energy, Reviews of Modern Physics **75**, 559 (2003).

[6] P. A. Ade *et al.* (Planck), Planck 2013 results. I. Overview of products and scientific results, Astronomy & Astrophysics **571**, A1 (2014).

[7] G. Bertone and D. Hooper, History of dark matter, Reviews of Modern Physics **90**, 045002 (2018).

[8] D. F. Jackson Kimball and K. van Bibber, The search for ultralight bosonic dark matter (2022).

[9] A. H. Guth, The Inflationary Universe: A Possible Solution to the Horizon and Flatness Problems, Phys. Rev. D **23**, 347 (1981).

[10] A. A. Starobinsky, A New Type of Isotropic Cosmological Models Without Singularity, Phys. Lett. B **91**, 99 (1980).

[11] A. D. Linde, A New Inflationary Universe Scenario: A

Parameter	Value	Units
Temperature, T	190	°C
K-^{3}He spin exchange cross section rate, $\kappa_{\mathrm{K-He}}$	$5.5 \cdot 10^{-20}$	cm^3/s
K-^{21}Ne spin exchange cross section rate, $\kappa_{\mathrm{K-Ne}}$	$3 \cdot 10^{-20}$	cm^3/s
K-^{3}He enhancement factor, $\lambda_{\mathrm{K-He}}$	$8\pi/3 \times 5.9$	
K-^{21}Ne enhancement factor, $\lambda_{\mathrm{K-Ne}}$	$8\pi/3 \times 30$	
K concentration, n_{K}	$9.7 \cdot 10^{13}$	cm^{-3}
^{3}He concentration, n_{He}	3.5	amg
^{21}Ne concentration, n_{Ne}	3.5	amg
Electron gyromagnetic ratio, γ_e	$2\pi \cdot 2.8$	MHz/G
^{3}He nuclear gyromagnetic ratio, γ_{He}	$2\pi \cdot 3.24$	kHz/G
^{21}Ne nuclear gyromagnetic ratio, γ_{Ne}	$2\pi \cdot 0.337$	kHz/G
K magnetic moment, μ_{K}	$9.274 \cdot 10^{-21}$	erg/G
^{3}He magnetic moment, μ_{He}	$1.154 \cdot 10^{-3} \mu_{\mathrm{K}}$	erg/G
^{21}Ne magnetic moment, μ_{Ne}	$0.359 \cdot 10^{-3} \mu_{\mathrm{K}}$	erg/G
K relaxation rate, Γ_{K}	600	Hz
^{3}He relaxation rate, Γ_{He}	$5 \cdot 10^{-5}$	Hz
^{21}Ne relaxation rate, Γ_{Ne}	$5 \cdot 10^{-5}$	Hz
Optimal pumping rate, $R_{p,\mathrm{K}}$	600	Hz
Low pumping rate, $R_{p,\mathrm{K}}$	60	Hz
K nuclear slowing-down factor, q_{K}	5.2	

TABLE I. Simulation parameters.

Nucleus	σ_n	σ_p	Refs.
^{3}He	0.87	−0.027	[39, 41]
^{21}Ne	0.196	0.013	[42]
^{39}K	0.034	−0.131	[39, 43]

TABLE II. Fractions of the nuclear spin due to neutron and proton spins. While the ^{3}He numbers are based on a full-scale shell model calculation and the ^{39}K numbers are based on a detailed perturbation theory calculation, the numbers for ^{21}Ne are estimates based on mirror nucleus properties and might not be as accurate, with other approaches giving different predictions [44].

	red circle	alternative
P_x^O	2.49	1.03
P_x^L	2.77	1.14

TABLE III. Responses (in arbitrary units) of the ^{39}K-^{3}He comagnetometers from Fig. 4 with the optimal pumping rate (P_x^O) and low pumping rate (P_x^L), for the point indicated by the red circle and the other point that gives the same ratio of responses. Since the values are different, their ratios with the response of any of the ^{39}K-^{21}Ne comagnetometers will be different, which will allow resolving the ambiguity.

Possible Solution of the Horizon, Flatness, Homogeneity, Isotropy and Primordial Monopole Problems, Phys. Lett. B **108**, 389 (1982).

[12] Y. Akrami *et al.* (Planck), Planck 2018 results. X. Constraints on inflation, Astron. Astrophys. **641**, A10 (2020), arXiv:1807.06211 [astro-ph.CO].

[13] R. L. Workman *et al.* (Particle Data Group), Review of Particle Physics, Section 90: Axions and Other Similar Particles, PTEP **2022**, 083C01 (2022).

[14] S. Weinberg, A new light boson?, Physical Review Letters **40**, 223 (1978).

[15] L. Di Luzio, B. Gavela, P. Quilez, and A. Ringwald, Dark matter from an even lighter QCD axion: trapped misalignment, Journal of Cosmology and Astroparticle Physics **10**, 001, arXiv:2102.01082 [hep-ph].

[16] A. Papageorgiou, P. Quílez, and K. Schmitz, Axion dark matter from frictional misalignment, Journal of High Energy Physics **01**, 169 (2023), arXiv:2206.01129 [hep-ph].

[17] K. Choi, S. H. Im, H. J. Kim, and H. Seong, Axion dark matter with thermal friction, Journal of High Energy Physics **02**, 180 (2023), arXiv:2206.01462 [hep-ph].

[18] M. Safronova, D. Budker, D. DeMille, D. F. Jackson Kimball, A. Derevianko, and C. W. Clark, Search for new physics with atoms and molecules, Reviews of Modern Physics **90**, 025008 (2018).

[19] M. Jiang, H. Su, A. Garcon, X. Peng, and D. Budker, Search for axion-like dark matter with spin-based amplifiers, Nature Physics **17**, 1402 (2021).

[20] M. Pospelov, S. Pustelny, M. Ledbetter, D. F. Jackson Kimball, W. Gawlik, and D. Budker, Detecting domain walls of axionlike models using terrestrial experiments, Physical Review Letters **110**, 021803 (2013).

[21] H. Masia-Roig, J. A. Smiga, D. Budker, V. Dumont, Z. Grujic, D. Kim, D. F. Jackson Kimball, V. Lebedev, M. Monroy, S. Pustelny, *et al.*, Analysis method for detecting topological defect dark matter with a global magnetometer network, Physics of the Dark Universe **28**, 100494 (2020).

[22] L. Darmé, L. Di Luzio, M. Giannotti, and E. Nardi, Selective enhancement of the QCD axion couplings, Phys. Rev. D **103**, 015034 (2021), arXiv:2010.15846 [hep-ph].

[23] F. Capozzi and G. Raffelt, Axion and neutrino bounds improved with new calibrations of the tip of the red-giant branch using geometric distance determinations, Phys. Rev. D **102**, 083007 (2020), arXiv:2007.03694 [astro-ph.SR].

[24] M. V. Beznogov, E. Rrapaj, D. Page, and S. Reddy, Constraints on Axion-like Particles and Nucleon Pairing in Dense Matter from the Hot Neutron Star in HESS J1731-347, Phys. Rev. C **98**, 035802 (2018), arXiv:1806.07991 [astro-ph.HE].

[25] S. Afach *et al.* (GNOME), What can a GNOME do? Search targets for the Global Network of Optical Magnetometers for Exotic physics searches, Annalen der Physik **2023**, 2300083 (2023), arXiv:2305.01785 [hep-ph].

[26] W. Terrano and M. Romalis, Comagnetometer probes of dark matter and new physics, Quantum Science and Technology **7**, 014001 (2021).

[27] I. M. Bloch, Y. Hochberg, E. Kuflik, and T. Volansky, Axion-like Relics: New Constraints from Old Comagnetometer Data, Journal of High Energy Physics **01**, 167 (2020), arXiv:1907.03767 [hep-ph].

[28] T. Wu, J. W. Blanchard, G. P. Centers, N. L. Figueroa, A. Garcon, P. W. Graham, D. F. Jackson Kimball, S. Rajendran, Y. V. Stadnik, A. O. Sushkov, *et al.*, Search for axionlike dark matter with a liquid-state nuclear spin comagnetometer, Physical Review Letters **122**, 191302 (2019).

[29] D. F. Jackson Kimball, D. Budker, T. E. Chupp, A. A. Geraci, S. Kolkowitz, J. T. Singh, and A. O. Sushkov, Probing fundamental physics with spin-based quantum sensors, Phys. Rev. A **108**, 010101 (2023).

[30] E. Klinger, T. Liu, M. Padniuk, M. Engler, T. Kornack, S. Pustelny, D. F. Jackson Kimball, D. Budker, and A. Wickenbrock, Optimization of nuclear polarization in an alkali-noble gas comagnetometer, Phys. Rev. Appl. **19**, 044092 (2023).

[31] M. Padniuk, M. Kopciuch, R. Cipolletti, A. Wickenbrock, D. Budker, and S. Pustelny, Response of atomic spin-based sensors to magnetic and nonmagnetic perturbations, Scientific Reports **12**, 324 (2022).

[32] T. G. Walker and W. Happer, Spin-exchange optical pumping of noble-gas nuclei, Reviews of Modern Physics **69**, 629 (1997).

[33] E. Babcock, I. Nelson, S. Kadlecek, B. Driehuys, L. Anderson, F. W. Hersman, and T. G. Walker, Hybrid spin-exchange optical pumping of ^{3}He, Physical Review Letters **91**, 123003 (2003).

[34] I. M. Savukov, Spin exchange relaxation free (SERF) magnetometers, in *High Sensitivity Magnetometers* (Springer, 2017) pp. 451–491.

[35] D. F. Jackson Kimball, J. Dudley, Y. Li, S. Thulasi, S. Pustelny, D. Budker, and M. Zolotorev, Magnetic shielding and exotic spin-dependent interactions, Physical Review D **94**, 082005 (2016).

[36] M. Padniuk, E. Klinger, G. Lukasiewicz, D. Gavilan-Martin, T. Liu, S. Pustelny, D. F. J. Kimball, D. Budker, and A. Wickenbrock, Universal determination of comagnetometer response to spin couplings, arXiv preprint arXiv:2309.16000 (2023).

[37] F. Le Kien, P. Schneeweiss, and A. Rauschenbeutel, Dynamical polarizability of atoms in arbitrary light fields: general theory and application to cesium, The European Physical Journal D **67**, 1 (2013).

[38] V. Dzuba, J. Berengut, J. Ginges, and V. Flambaum, Screening of an oscillating external electric field in atoms, Physical Review A **98**, 043411 (2018).

[39] D. F. Jackson Kimball, Nuclear spin content and constraints on exotic spin-dependent couplings, New Journal of Physics **17**, 073008 (2015).

[40] H. Masia-Roig *et al.*, Intensity interferometry for ultralight bosonic dark matter detection, Phys. Rev. D **108**, 015003 (2023), arXiv:2202.02645 [hep-ph].

[41] J. L. Friar, B. F. Gibson, G. L. Payne, A. M. Bernstein, and T. E. Chupp, Neutron polarization in polarized ^{3}He targets, Phys. Rev. C **42**, 2310 (1990).

[42] J. Engel and P. Vogel, Spin dependent cross-sections of weakly interacting massive particles on nuclei, Phys. Rev. D **40**, 3132 (1989).

[43] J. Engel, M. T. Ressell, I. S. Towner, and W. E. Ormand, Response of mica to weakly interacting massive particles, Phys. Rev. C **52**, 2216 (1995), arXiv:hep-ph/9504322.

[44] Y. V. Stadnik and V. V. Flambaum, Nuclear spin-dependent interactions: Searches for WIMP, Axion and Topological Defect Dark Matter, and Tests of Fundamental Symmetries, Eur. Phys. J. C **75**, 110 (2015), arXiv:1408.2184 [hep-ph].